PERFORMANCE IMPROVEMENT OF POLYMER ELECTROLYTE MEMBRANE FUEL CELLS BY BIPOLAR PLATE MODIFICATION USING COMPUTATIONAL FLUID DYNAMICS.

[1]Ovais Shaikh, [2]Prof V.B.Sawant

[1] Research Student, [2]Assisstant Professor,
[1]Faculty of Mechanical Engineering,
Rajiv Gandhi Institute of Technology, Mumbai, India.

Abstract : Bipolar plates are one of the most important functional element of Polymer Electrolte Membrane Fuel Cell (PEMFC). They provide separate gas flow channels that provide supply of reactant gases on anode and cathode electrode sides of fuel cell and facilitate removal of products from the cathode side of fuel cell. A three dimensional single phase numerical model is proposed in this work based on Fluent PEMFC Module to study conventional flow field patterns of serpentine, interdigitated, mesh type and parallel flow fields used in bipolar plates. The model is validated by comparison with published experimental results. Based on the results obtained it was found interdigitated flow field gave the best performance followed by serpentine, parallel and pin type flow fields respectively. Hence, a new hybrid design using a combination of interdigitated and serpentine field was developed and simulated. In terms of power density, the hybrid flow field outperforms all the conventional flow fields. Hybrid field showed higher pressure drop in comparison to conventional flow fields thus resulting in high pumping power.

IndexTerms **- Polymer Electrolyte Membrane Fuel Cell (PEMFC), hybrid, Power density, Current density, Voltage.**

I. INTRODUCTION

A fuel cell is an electrochemical device that converts chemical energy of fuel into electrical energy.Among different types of fuel cells, Polymer Electrolyte Membrane Fuel Cell (PEMFC) in the recent years have been widely used as an attractive source for power generation,an alternative to fossil fuels and internal combustion engines. Coupled with advantages of high efficiency, low operating temperature and low emission there are other obstacles such as high cost and poor performance at higher current densities[22].

The major components of PEMFC are: Anode Side, Cathode Side and Membrane Electrode Assembly (MEA) sandwiched between them. The anode and cathode side consists of the Anode Terminal and the Cathode Terminal respectively or the Current Collector Plate also known as the bipolar plates. The MEA consists of the membrane which acts as the electrolyte. Hydrogen and air/oxygen are fed to the anode and cathode side electrodes respectively which result in the following electrochemical reactions on the anode and cathode sides:

Anode Side:

$$H_2 \rightarrow 2H^+ + 2e^- \quad (1.1)$$

Cathode Side:

$$\tfrac{1}{2} O_2 + 2H^+ + 2e^- \rightarrow H_2O \quad (1.2)$$

Bipolar plates form one of the key components of PEMFC and perform important functions such as supplying and distribution of reactant gases on cathode and anode sides as well as acting as current collectors[6-23].

Xianguo Li et al**.** [22] provided a comprehensive review of conventional flow field designs of bipolar plate in PEM fuel cells. A pin type flow field network formed by many pins arranged in a sequential pattern results in a low reactant pressure drop, however it may lead to the channeling and formation of stagnant areas across the low resistance path. This may lead to uneven reactant distribution, inadequate product water removal and poor fuel cell performance. This problem of stagnation areas is overcome by the use of serpentine flow fields which forces the reactant to travel the entire area of flow path. However the length of flow path is increased which results in an increased pressure drop and concentration gradients in the flow channels. A parallel flow field is similar to the pin type flow field except for the fact that parallel type flow fields have straight land areas separated by grooves which force the reactant to flow in parallel directions. The similarity in design to pin type flow fields yields the same problems as those encountered by the pin type flow field leading to channeling and formation of stagnant areas.

A number of studies were conducted to assess the performance of fuel cells using different flow channels. Ferng [23] studied parallel and serpentine multipath flow channels with uniform depth and stepwise depth using a three dimensional CFD Model. Serpentine channels performed better as compared to parallel channels in this model. A study was conducted by Hashemi et al. [9] on a non isothermal 3 dimensional model which involved serpentine and parallel flow fields. They concluded that serpentine field performed better than parallel flow field in terms of current density distribution and temperature. Different dynamics were considered in design of serpentine flow fields with Jeon et al. [7] considering single channel, double channel, cyclic single channel, and symmetric single channels of serpentine flow fields. Low pressure drop was observed for cyclic single channel and symmetric single channel flow fields. It was concluded that these flow fields would be advantageous for larger scale system and low inlet humidity operations.

Interdigitated flow field consists of dead end channels i.e inlet and outlet of flow field are not connected for fluid flow. Rather the fluid diffuses through the gas diffusion layer in the MEA under pressure with convection velocity. This convection velocity helps in water removal from the membrane electrode assembly, but slowness of this convective diffusion leads to large

concentration gradients across the MEA and the bipolar plate. Xianguo Li et al. [22] have reported that interdigitated flow fields provide the highest power output of all the conventional flow fields.

Recently newly designed flow fields other than conventional flow fields have been employed for research purposes. Various innovations in the form of constructal theory and bio – inspired form have been employed for flow field design. These designs provide advantages as well as disadvantages over the conventional flow fields. Gutierrez et al. [6] employed a tree shaped design for flow distribution in PEMFC. They employed different bifurcation patterns as appearing in branches of trees namely level one, two and three for bifurcations respectively. The three level bifurcation showed highest power output as it had the most utilization of membrane active area. Power density obtained was less than serpentine but more than parallel flow channel. Another bio – inspired pattern was developed by Roshandel et al. [19]. The design showed higher power output and more uniform velocity and molar concentration distribution of reactant species.

Of all the flow fields analyzed using the numerical model interdigitated flow fields provided the highest power output followed by serpentine flow field. The present study aims at developing a new hybrid flow field by carrying out a modification of conventional interdigitated and serpentine flow field. The study aimed at using different geometries of flow paths for carrying the cathodic and anodic species. The objective of the present study is to provide a comparison of new hybrid flow fields with the conventional flow fields in terms of different parameters such as current density, power output and molar concentration distribution.

II. HYBRID FLOWFIELD DESIGN

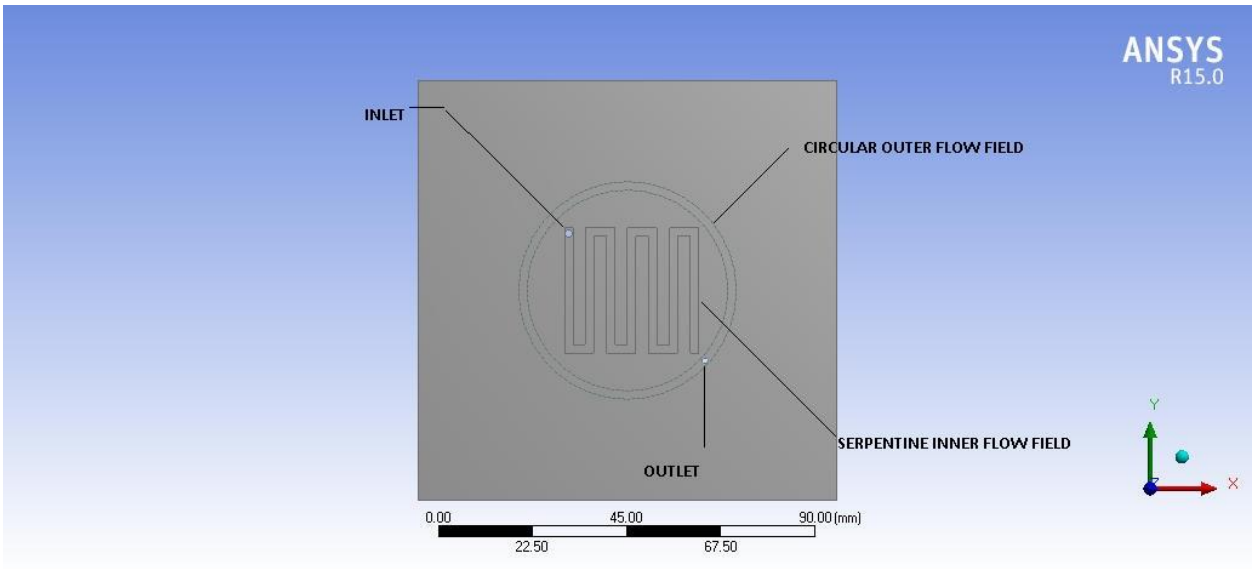

Fig 1: Hybrid flow field design

As shown in figure 1, the design consists of an inlet inner serpentine flow channel with inlet manifold. The reactant gas enters through this inlet flow channel and flows the entire channel upto its dead end. The reactant gas then diffuses into Membrane Electrode Assembly through molecular diffusion and reaches the outer circular flow field with dead end at one end and outlet manifold at the other end. This type of design increases the net available active Membrane Area which provides for better utilization of Membrane Electrode Assembly for electrochemical reactions.

The present study uses a single phase and three dimensional model for the above mentioned hybrid flow field design of PEMFC. The model takes into account the surface overpotential i.e difference between phase potential of solid and electrolyte/membrane. The potential equations account for electron transport through the current collectors and protonic transport of electrolytic ions. The model was validated with published experimental results to verify its accuracy.

III. MODEL DESCRIPTION

This study presents a three dimensional PEMFC steady state model with following assumptions:

- The flow is laminar.
- The fluid is incompressible.
- The inlet gases follow the ideal gas law.
- The gas diffusion layers, catalyst layers and membrane are assumed to be isotropic materials.
- Steady State conditions exist.
- Isothermal conditions exist across the fuel cell.
- The membrane is proton conductive but impermeable to diffusion of reactant gases.

3.1 Governing Equations

The flow channel geometry influences the reactant transport which is governed by the mass conservation equation given as:

$$\frac{\partial \rho}{\partial t} + \nabla.(\rho v) = S_m \qquad (3.1)$$

Where is v is the velocity vector and S_m is the mass source term. The term ρ represents the scalar density and operator ∇ represents the partial derivative in Cartesian co-ordinates defined as $\frac{d}{dx}i + \frac{d}{dy}j + \frac{d}{dz}k$. The source term is assumed to be zero in flow channels, gas diffusion layers and membranes. The source term is not zero in the catalyst layers because of

the electrochemical reactions occurring at this zone. The mass consumption rates of hydrogen and oxygen per unit volume are given by:

$$S_{H_2} = -\frac{M_{wH_2} R_{an}}{2F} < 0 \quad (3.2)$$

$$S_{O_2} = -\frac{M_{wO_2} R_{cat}}{4F} < 0 \quad (3.3)$$

The mass consumption rate of water per unit volume is given by:

$$S_{H_2O} = -\frac{M_{wH_2O} R_{cat}}{2F} > 0 \quad (3.4)$$

The momentum equation solves for the fluid velocities in the channels and gas diffusion layers and for the species' partial pressure.

$$\frac{\partial \rho v}{\partial t} + \nabla.(\rho v v) = -\nabla p + \nabla.\tau + S_{mom} \quad (3.5)$$

Here τ stands for shear tensor and S_{mom} stands for momentum source term. The momentum source term is set to be zero in the flow channel and membrane and considered in the diffusion layer and catalyst layer as follows:

$$S_{mom} = -\frac{\mu_i}{k.k_r} v \quad (3.6)$$

For the liquid phase k_r is

$$k_r = s^3 \quad (3.7)$$

For the gaseous phase, k_r is

$$k_r = (1-s)^3 \quad (3.8)$$

In these equations, s is the liquid water saturation, k is absolute permeability and k_r is relative permeability.

The conservation of species is required to calculate the mass balance for each of the involved reactants in the current study and is defined as follows:

$$\frac{\partial(\epsilon \rho y_j)}{\partial t} + \nabla.(\rho v y_i) = \nabla.\left(\rho D_j \nabla y_i\right) + S_j \quad (3.9)$$

The effective mass diffusivity is calculated according to equation

$$D_j = \epsilon^{1.5}(1-s)^{2.5} D_j^o \left(\frac{p_0}{p}\right)^1 \left(\frac{T}{T_0}\right)^{1.5} \quad (3.10)$$

Here s which is the liquid water saturation is zero because the current model is assumed to be single phase.D_i^0 is the reference diffusivity based on reference pressure p_0 and reference temperature T_0. The gas diffusion and catalyst layer is assumed to be homogenous porous media and fluid flow in porous media is modeled by Darcy's law as follows:

$$v = -\left(\frac{k_p}{\mu_i}\right) \nabla p \quad (3.11)$$

The effective gas species diffusivity can be calculated using the following equation by accounting for porous media tortuosity.

$$D_j^{eff} = \epsilon^{1.5} D_j \quad (3.12)$$

The energy equation can be written as

$$\nabla.(\rho_i v T) = \nabla.(k^{eff}.\nabla T) + S_h \quad (3.13)$$

Here k^{eff} is the effective heat conductivity in porous media which is calculated as

$$k^{eff} = \epsilon k_f + (1-\epsilon) k_s \quad (3.14)$$

Where k_f and k_s are liquid and solid conductivity in porous media respectively.

In the energy equation S_h is the heat source which can be estimated by

$$S_h = h_{phase} + h_{reaction} + I^2 R_{ohm} + R_{an,cat}\eta_{an,cat} \quad (3.15)$$

Where $h_{reaction}$ is the net enthalpy change due to electrochemical reactions, $R_{an,cat}\eta_{an,cat}$ is the product of the transfer current and the overpotential in the anode or cathode catalyst layer, R_{ohm} is the ohmic resistivity of conducting media and h_{phase} is the enthalpy change due to condensation/ vaporization of water.

The computational rates of anodic and cathodic reactions forms the basis of electrochemistry model adopted by the current study. The principle on which the reaction works is the surface overpotential i.e the difference between the phase potential of solid and phase potential of electrolyte/membrane. One potential equation accounts for the electron transport through solid conductive materials (current collectors and solid grids of porous media).

$$\nabla.(\sigma_{sol} \nabla \phi_{sol}) + R_{sol} = 0 \quad (3.16)$$

Where σ_{sol} is the ionic conductivity of electrodes and ϕ_{sol} is the potential in electrodes , R_{sol} is the volumetric transfer current (A/m^3) at the anode and cathode catalyst layers defined by :

$$R_{sol} = -i_a \quad (3.17)$$

At the anodic side, and

$$R_{sol} = +i_c \quad (3.18)$$

At the cathodic side.

The charge balance in the membrane is given by other potential equation which also represents the protonic transport of H^+ or O^{2-}.

$$\nabla.(\sigma_{mem} \nabla \phi_{mem}) + R_{mem} = 0 \quad (3.19)$$

Where σ_{mem} is the ionic conductivity of membrane, ϕ_{mem} is membrane potential and R_{mem} is the volumetric transfer current (A/m^3) which is defined by:

$$R_{mem} = i_a \quad (3.20)$$

At the anodic side, and

$$R_{mem} = -i_c \quad (3.21)$$

At the cathodic side.

The membrane conductivity is a function of membrane water content, λ and is calculated as :

$$\sigma_{mem} = (0.514\lambda - 0.326).\exp\left[1268\left(\frac{1}{303} - \frac{1}{T}\right)\right] \quad (3.22)$$

The water content of membrane is calculated by:

$$\lambda = \frac{EW_M.C_W}{\rho_m.M_{H_2O}} \quad (3.23)$$

Where ρ_m is the density of dry membrane and EW_M is the equivalent molecular weight of the membrane.

The terms in the equations which are also known as source transfer currents are calculated by using Butler-Volmer Equation as follows:

$$i_a = \left(\tau_{an} j_{an}^{ref}\right)\left([A]/[A]_{ref}\right)^{\gamma_{an}}\left(e^{\frac{\alpha_{an}F\eta_{an}}{RT}} - e^{\frac{-\alpha_{cat}F\eta_{an}}{RT}}\right) \quad (3.24)$$

$$i_c = \left(\tau_{cat} j_{cat}^{ref}\right)\left([C]/[C]_{ref}\right)^{\gamma_{cat}}\left(-e^{\frac{\alpha_{an}F\eta_{cat}}{RT}} + e^{\frac{-\alpha_{cat}F\eta_{cat}}{RT}}\right) \quad (3.25)$$

Here j_{an}^{ref} =reference exchange current density per active surface area (A/m^2)

τ =specific active surface area (1/m)

[ ],[ ]$_{ref}$=local species concentration, reference value (kmol/m^3)

γ=Concentration dependence

α=transfer coefficient (dimensionless)

F=Faraday Constant (9.65 x 10^7 C/kmol)

The driving force for the kinetics is the local surface overpotential, η, also known as the activation loss . It is generally the difference between the solid and membrane potentials, ϕ_{sol} and ϕ_{mem}.

$$\eta_{an} = \phi_{sol} - \phi_{mem} \quad (3.26)$$

The gain in electric potential from crossing from the anode side to cathode side can then be taken into account by subtracting the open circuit voltage V_{oc} on the cathode side.

$$\eta_{cat} = \phi_{sol} - \phi_{mem} - V_{oc} \quad (3.27)$$

The open circuit voltage can be calculated as :

$$V_{OC} = 1.229 - 0.9\ x\ 10^{-3}(T - 298) + 2.3\ \frac{RT}{4F}\log(P_{H_2}^2\ P_{O_2}) \quad (3.28)$$

This equation can also be written as:

$$V_{OC} = 0.2329 + 0.0025\ x\ T \quad (3.29)$$

3.2 Boundary Conditions

The boundary conditions applied are shown in Table 1.

Table 3.1: Boundary Conditions

Boundary	Anode inlet	Anode Outlet	Cathode inlet	Cathode Outlet	Anode terminal	Cathode terminal
Mass flow rate (kg/s)	5.19x10^{-6}	-	1.28x10^{-4}	-	-	-
Temperature (K)	353	353	353	353	353	353
Species Mass Fraction O_2	0	0	0.2	0	-	-
Species Mass Fraction H_2	0.3	0	0	0	-	-
Species Mass Fraction H_2O	0.7	0	0.14	0	-	-
Pressure Outlet (atm)	-	1	-	1	-	-
Electrode Potential	$\frac{\partial\phi_{sol}}{\partial z} = 0$	$\frac{\partial\phi_{mem}}{\partial z} = 0$	$\frac{\partial\phi_{sol}}{\partial z} = 0$	$\frac{\partial\phi_{sol}}{\partial z} = 0$	$\phi_{sol} = 0$	$\phi_{sol} = V_{cell}$
Membrane Potential	$\frac{\partial\phi_{mem}}{\partial z} = 0$	$\frac{\partial\phi_{mem}}{\partial z} = 0$	$\frac{\partial\phi_{mem}}{\partial z} = 0$	$\frac{\partial\phi_{mem}}{\partial z} = 0$	$\frac{\partial\phi_{mem}}{\partial z} = 0$	$\frac{\partial\phi_{mem}}{\partial y} = 0$

3.3 Numerical Solution

The numerical solution was obtained by solving governing equations of momentum, species and mass transport using Finite Volume Method. In this work, a circular path was present in the flow field which places the current work in recirculating flow problems. Hence as reported by Rostami et al. [13] for recirculating flow problem SIMPLEC Algorithm was used which was

more economic for such type of problems. Also first order methods were used for solving species and mass transport equations. Under relaxation factors were pressure (0.3), momentum (0.6), water content (0.95) to achieve specific convergence criteria which was set at 10^{-5} iterations for momentum, species mass fractions, electronic potential, protonic potential and energy equation. Grid independence test was carried out at cell voltage V=0.7 V and 70000 nodes were considered as threshold for obtaining grid independence.

IV. RESULTS AND DISCUSSION

4.1 Validation of Numerical Model

The results obtained from numerical model were compared with the experimental results obtained from Siegel et al. [16]. The results showed good agreement with experimental values in the region between higher and lower current densities. At higher and lower current densities the curve shows linear characteristics and consequently higher values than actual values. The actual values to be obtained in polarization curves are lower as water accumulation in Catalayst layer and Gas diffusion layer causes a resistance to mass flow of reactants decreasing the fuel cell performance. The model used in the present study is a single phase model where the generated water is transported as vapor. Hence this single phase model results in linear current density along the gas channel.

4.2 Concentration distribution of Hydrogen and Current density distribution

Molar concentration distribution of hydrogen for hybrid design is shown. There is a decrease in hydrogen concentration from inlet to outlet. Membrane concentration of hydrogen shows a uniform distribution from inlet to outlet portion of the membrane. Consequently membrane shows an increase in hydrogen concentration distribution at the edges whereas the hydrogen concentration at the flow field area decreases as the hydrogen is consumed in the electrochemical reactions.

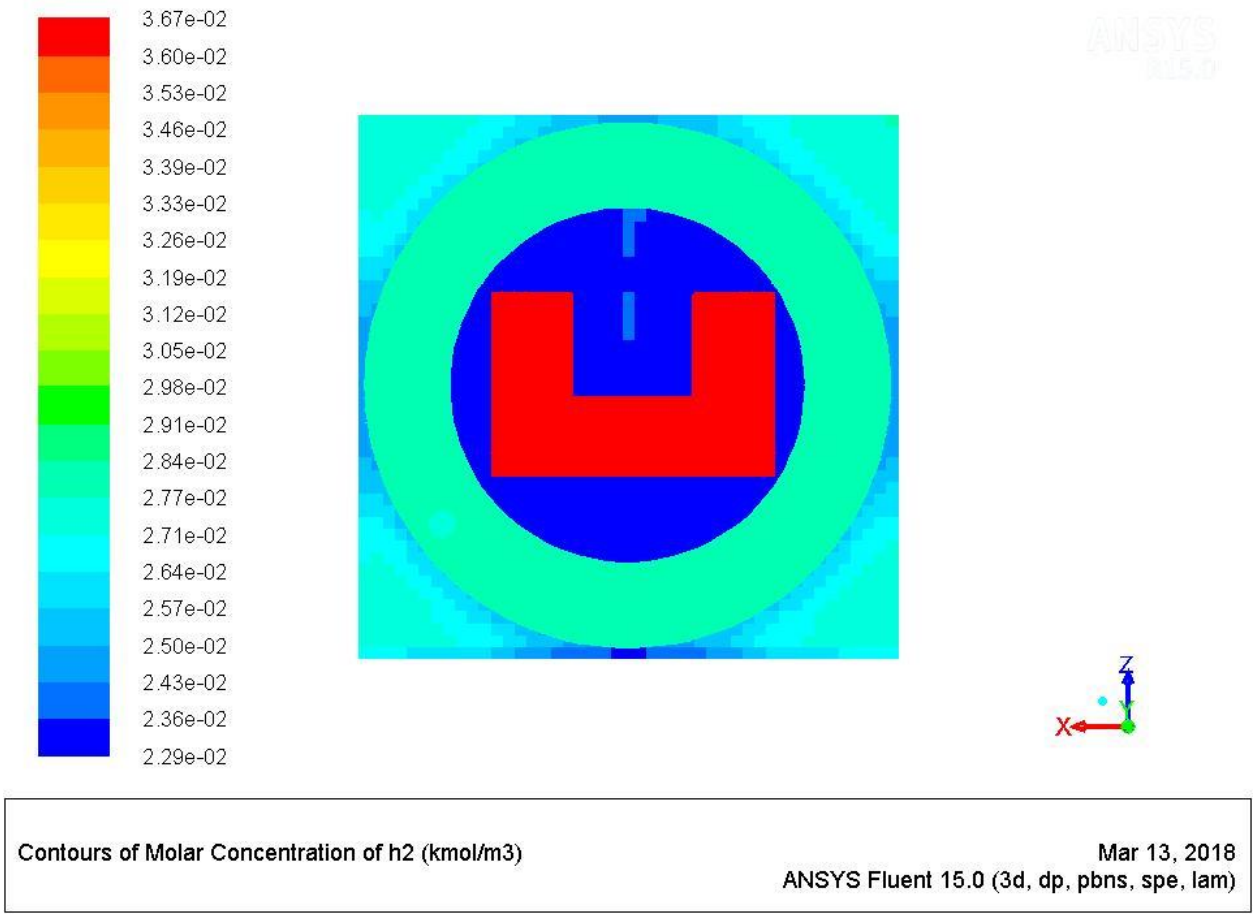

Fig 2 : Molar concentration of H_2

Current density distribution for V=0.7 V for hybrid design is shown in figure 2. Current density distribution depends on the active area of fuel cell and its utilization. The fig shows that almost entire area is utilized for generation of current which results in higher current and power density of the fuel cell. Also the fig shows that current density decreases from inlet to outlet as reactants are consumed as they traverse from inlet to outlet. The area of minimum current generation is almost negiligible in this type of design, thus making it an attractive choice for higher power generation and improving the overall fuel cell performance.

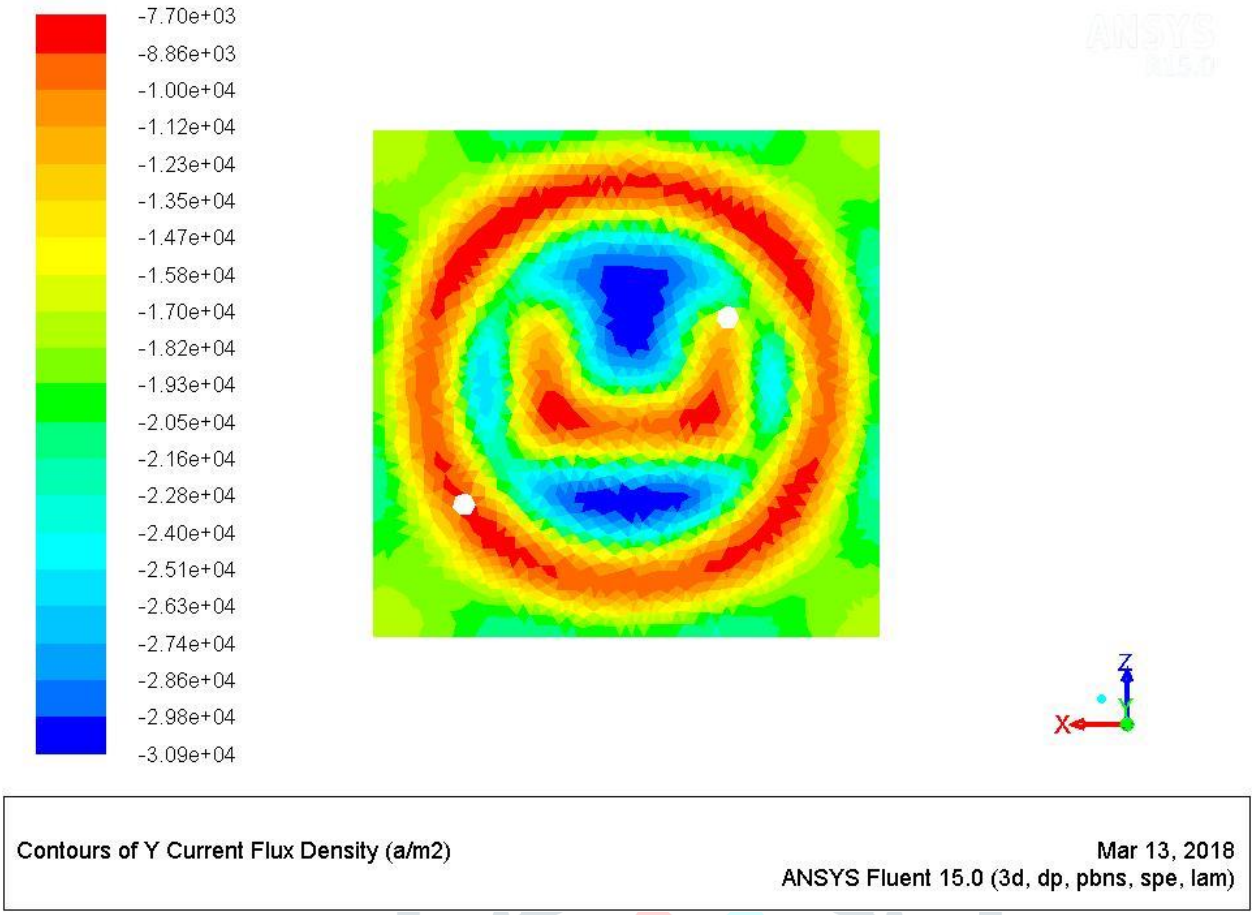

Fig 3: Current Density Distribution in Hybrid Design.

4.3 Performance Comparison with Conventional flow fields

A comparison is performed between the hybrid flow fields and the conventional flow fileds. All the four conventional flow fields namely serpentine, pin type, parallel and interdigitated are simulated with same geometrical and numerical conditions. The numerical results obtained are compared with the hybrid flow field design. Power density comparisons are shown in the figure 4.

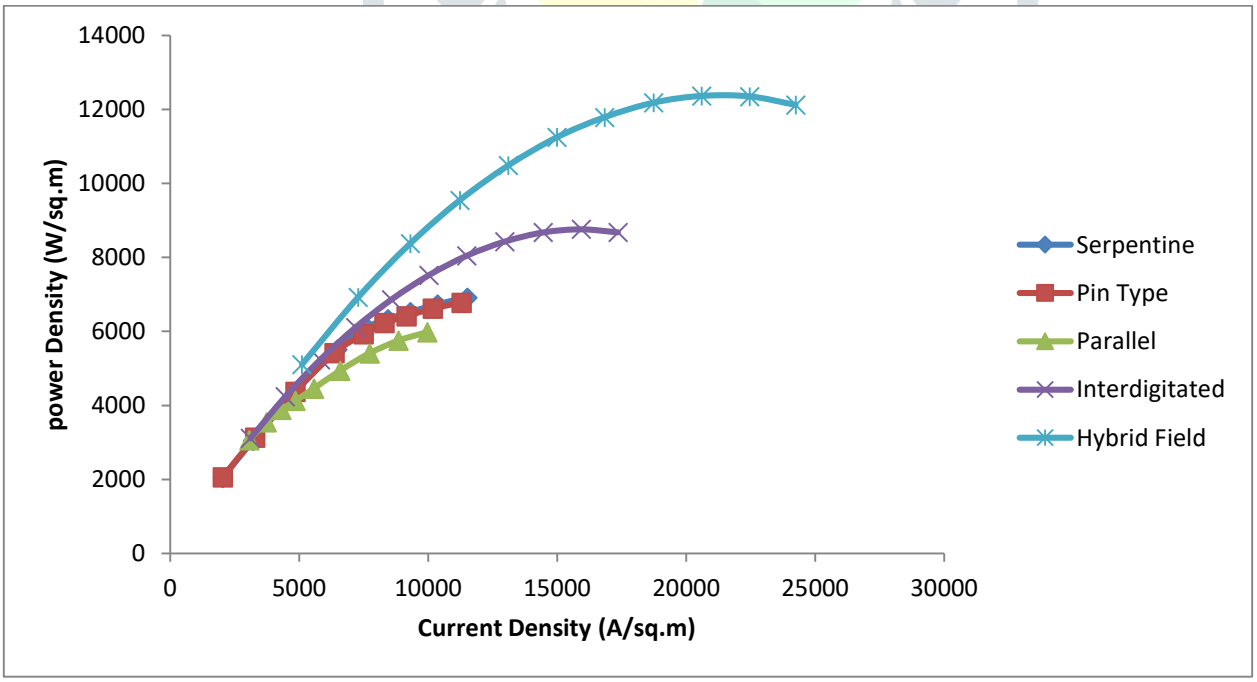

Fig 4: Power density comparisons for different flow fields

The figure 4 shows highest power density for hybrid flow field followed by interdigitated and serpentine flow field. Pin type flow field shows higher power density as compared to parallel flow field which shows the least power density of all the flow fields. The reason for obtaining higher power density for hybrid flow field is due to proper utilization of active area of fuel cell. A comparison of current density distribution shown in figure 5 shows that hybrid flow field has the least unutilized active area as compared to other conventional flow fields.

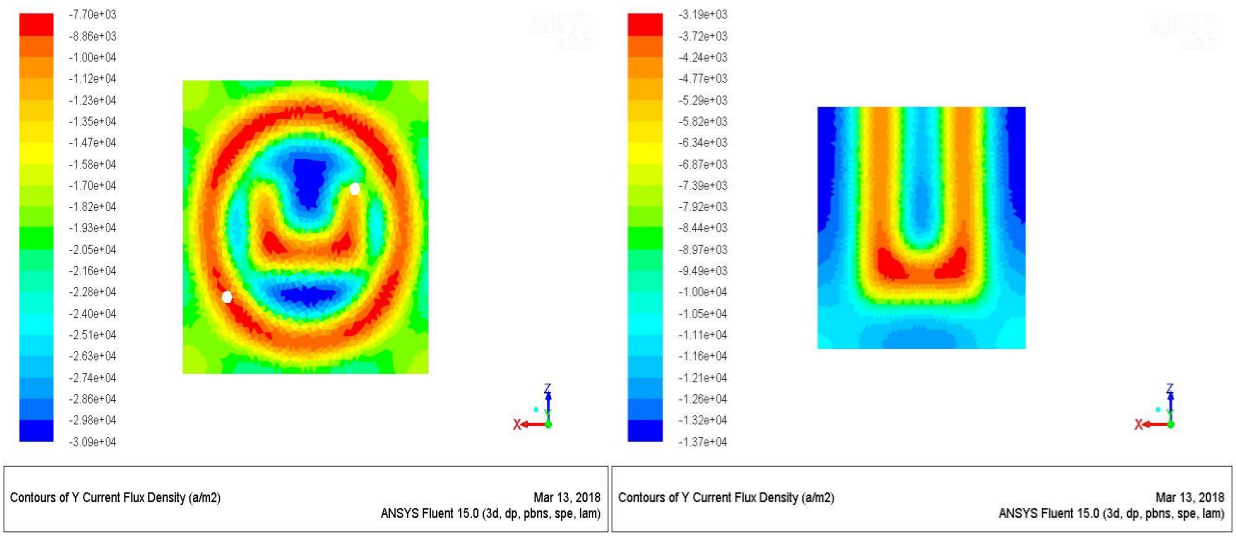

(a) (b)

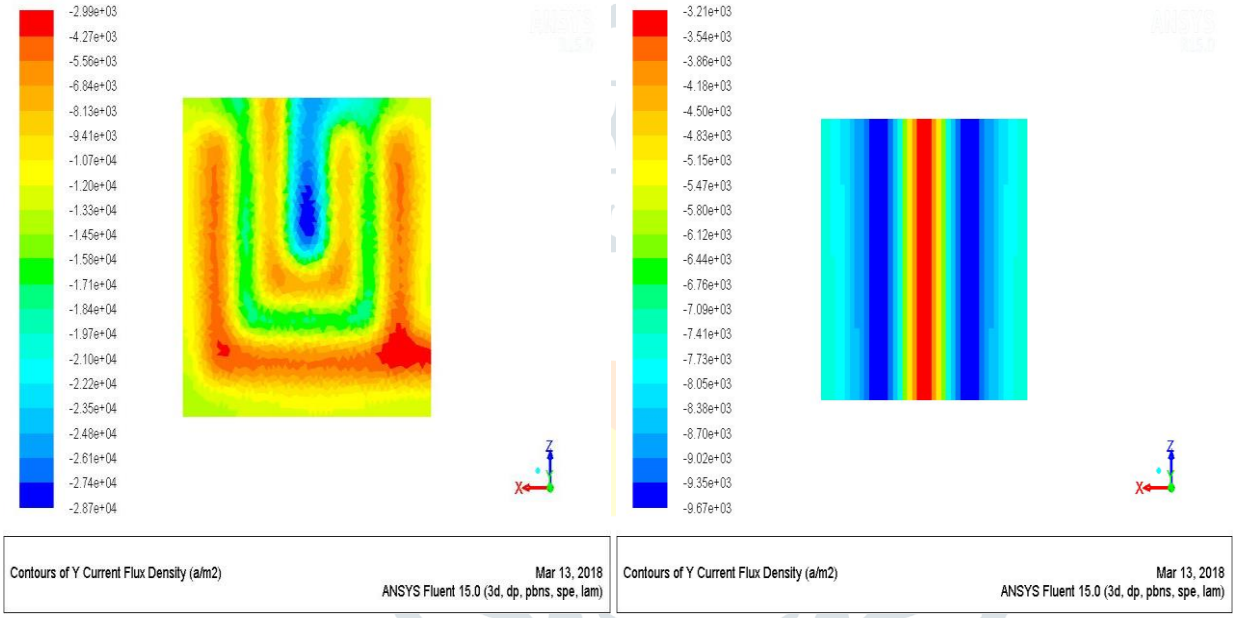

(c) (d)

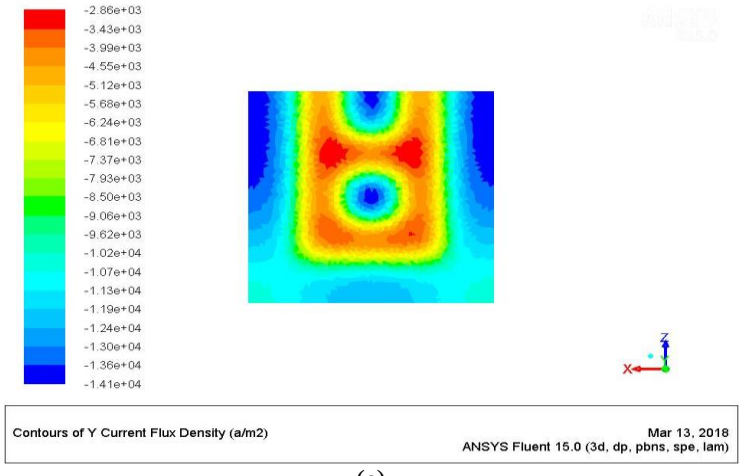

(e)

Fig 5 : Current Density Distribution for (a) Hybrid Flow Field, (b) Serpentine Flow Field, (c) Interdigitated Flow Field (d) Parallel Flow Field, (e) Pin Type Flow Field.

The table below shows maximum power densities of the conventional flow fields and their comparison with hybrid flow field.

Table 4.1: Comparison of Power Densities

Flow Field Type	Voltage (V) at which maximum Current Density is Obtained	Maximum Power Density (W/sq.m)	Hybrid Flow Field Power Density (W/sq.m)	Improvement by Hybrid Flow Field %
Serpentine	0.6	6913.1	12362.94	78.83
Interdigitated	0.55	8760.82	12350.58	40.98
Pin Type	0.6	6774.32	12362.94	82.5
Parallel	0.6	5980.14	12362.94	106.73

The maximum power densities of the hybrid flow field show an increase of 78.83 %, 40.98 %, 82.5 % and 106.73 % over serpentine, interdigitated, pin type and parallel flow fields respectively. The higher power densities of the hybrid flow field is due to more uniform current distribution across the flow field which results in an increase in power densities.

Pressure drop forms an important parameter in design of fuel cell as it powers the reactant distribution through the fuel cell. Pressure drop should be low as it facilitates reactant distribution which in turn increases the power density of fuel cell. However in this study hybrid flow field shows the highest pressure drop of 30.81 Pa between inlet and outlet. The conventional flow fields of serpentine, parallel, interdigitated and pin type show a pressure drop of 3.6 Pa, 3.5 Pa, 2.776 Pa and 3.55 Pa respectively. Inspite of highest pressure drop, the hybrid flow field shows highest power output for conventional flow field despite low pressure drops for the later. The majority of pressure drop in hybrid flow field is obtained at the inlet and outlet which have a mutually perpendicular direction to the flow channel. In order to provide a proper comparison between the net power output and pressure drops Daniel Lorenzini Gutierrez et al. determined net power as a function of difference between power density and net pumping power required to pump the reactants in the flow channel. The Pumping Power is a function of pressure drop developed in the flow channel. The table shows the net power developed considering the pumping power for each flow field at V=0.7 V.

Table 4.2: NET POWER DEVELOPED COMPARISON WITH LORENZINI GUITERREZ ET AL.[6]. (V=0.7V)

Type of flow field	**Pressure Drop(Pa)**	**Power Density(W/cm^2)**	**Pumping Power (W/cm^2)**	**Net Power(W/cm^2)**
Three levels of bifurcation	36.28	0.2968	1.4813×10^{-5}	0.2967
Serpentine	18011.78	0.4035	7.3542×10^{-3}	0.3961
Parallel	542.6	0.1972	2.2154×10^{-4}	0.1969
Hybrid flow field	30.81	1.1786	0.3327	0.8458

The above table shows that even with such a higher pressure drop and higher pumping power requirement the hybrid flow field produces more net power as compared to that by Guiterrez et al.[6].

V. CONCLUSIONS

The study of different type of flow fields in bipolar plates of a PEM Fuel cell is an important topic for analyzing overall performance of PEM Fuel Cell. This study presents a single phase PEM Fuel cell model based on FLUENT Module of ANSYS 15.0 and validated based on experimental results as reported by Siegel. The obtained results are in good agreement with experimental data. This project presents numerical analysis of conventional flow fields namely serpentine, interdigitated, parallel and pin type flow fields in terms of power densities and current densities. Power and current densities depend upon the effective utilization of membrane area and uniform flow distribution of reactants in flow fields.

The results show that hybrid flow field reported the highest values of power and current densities as compared to all other conventional flow fields. The reason for such higher values of current density being the larger area covered by the flow channels of the hybrid flow field whereas the unutilized areas decrease the net power output of fuel cell.

Power density analysis was performed considering the pressure drop which takes pumping power of reactants into consideration. Hybrid Flow field reported higher power densities as compared to all other conventional flow fields even after showing highest pressure drops.

In this study circular flow field was used to increase the overall area of flow channels through which the reactant flows. Hence future studies may provide an alternative to increase the flow field design in a way to better the performance provided by hybrid flow field. Some geometrical designs such as rectangular, trapezoidal, hexagonal or pentagonal areas can be used in place of circular flow fields to better the performance.

REFERENCES

[1] Abul Bashar Mahmud Hasan, "Experimental and numerical study of feeding channel in proton exchange membrane fuel cell", Bangladesh University of Engineering and Technology, 2005.

[2] Adam Arvay, "Proton Exchange Membrane Fuel Cell Modeling and Simulation using Ansys Fluent", Arizona State University.

[3] Anthony D. Santamaria, Nathanial J. Cooper, Maxwell K. Becton, Jae Wan Park, "Effect of channel length on interdigitated flow-field PEMFC performance: A computational and experimental study", International Journal of Hydrogen Energy 37, Pages 16253-16263, 2013.

[4] Bladimir Ramos-Alvarado, Abel Hernandez-Guerrero, Daniel Juarez-Robles, Peiwen Li , "Numerical investigation of the performance of symmetric flow distributors as flow channels for PEM fuel cells", International Journal of Hydrogen Energy 37, Pages 436-448, 2012.

[5] Daniel Juarez-Robles, Abel Hernandez-Guerrero, Bladimir Ramos-Alvarado, Francisco Elizalde-Blancas, Cesar E. Damian-Ascencio, "Multiple concentric spirals for the flow field of a proton exchange membrane fuel cell", Journal of power Sources 196, Pages 8019-8030, 2011.

[6] Daniel Lorenzini-Gutierrez, Abel Hernandez-Guerrero, Bladimir Ramos-Alvarado, Isaac Perez-Raya, Alejandro Alatorre-Ordaz, "Performance analysis of a proton exchang membrane fuel cell using tree-shaped designs for flow distribution", International Journal of Hydrogen energy 38, Pages 14750-14763, 2013.

[7] D.H. Jeon, S. Greenway, S. Shimpalee, J.W. Van Zee, "Effect of serpentine flow field design on PEM fuel cell performance", International Journal of Hydrogen Energy 33,Pages 1052-1066,2008.

[8] E. Planesa, L.Flandina, N.Alberola, "Polymer composite bipolar plates for PEMFC", Energy Procedia 20,Pages 311-323,2012..

[9] Fatemeh Hashemia, Soosan Rowshanzamira, Mashallah Rezakazemia, "CFD simulation of PEM fuel cell performance: Effect of straight and serpentine flow fields", Mathematical and Computer Modelling 55, Pages 1540-1557, 2012.

[10] Glenn Creighton Catlin, "PEM fuel cell modeling and optimization using a genetic algorithm", University of Delaware, 2010.

[11] Isanaka, Sriram Praneeth, Austin Das, and Frank Liou, "Design Of Metallic Bipolar Plates for Pem Fuel Cells", Center for Transportation Infrastructure and Safety/NUTC program Missouri University of Science and Technology.

[12] Hong Liu, Peiwen Li, Kai Wang, "Optimization of PEM fuel cell flow channel dimensions Mathematic modeling analysis and experimental verification", International Journal of Hydrogen Energy 38, Pages 9835-9846, 2013.

[13] Leila Rostami , Puriya Mohamad Gholy Nejad , Ali Vatani ," A numerical investigation of serpentine flow channel with different bend sizes in polymer electrolyte membrane fuel cells", International Journal of Hydrogen Energy 97,Pages 400-410,2016.

[14] Linfa Peng , Peiyun Yi , Xinmin Lai, "Design and manufacturing of stainless steel bipolar plates for PEM fuel cells:A review", International Journal of Hydrogen Energy,Pages 1-27,2014.

[15] M. ElSayed Youssef , R.S. Amin , K.M. El-Khatib , "Development and performance analysis of PEMFC stack based on bipolar plates fabricated employing different designs", Arabian Journal of Chemistry,2015.

[16] N.P. Siegel, M.W. Ellis, D.J. Nelson, M.R. von Spakovsky, "A two-dimensional computational model of a PEMFC with liquid water transport", Journal of Power Sources 128, Pages 173-184, 2004.

[17] Rajesh Boddu, Uday Kumar Marupakula, Benjamin Summers, Pradip Majumdar, "Development of bipolar plates with different flow channel configurations for fuel cells", Journal of Power Sources 189, Pages 1083-1092, 2009.

[18] Renato A. Antunesa, Mara C.L. de Oliveirab, Gerhard Ett ,Volkmar Ett, "Carbon materials in composite bipolar plates for polymer electrolyte membrane fuel cells: A review of the main challenges to improve electrical performance", Journal of Power Sources 196 ,Pages 2945-2961,2010.

[19] R. Roshandel, F. Arbabi, G. Karimi Moghaddam, "Simulation of an innovative flow-field design based on a bio inspired pattern for PEM fuel cells", Renewable Energy 41, Pages 86-95, 2012.

[20] Shou-Shing Hsieh, Yi-Ji Huang, Bing-Shyan Her, "Pressure drop on water accumulation distribution for a micro PEM fuel cell with different flow field plates", International Journal of Heat and Mass Transfer 52, Pages 5657-5659, 2009.

[21] Travis Lee Smitha ,Anthony D. Santamariaa, Jae Wan Parka, Kazuo Yamazakia, "Alloy selection and die design for stamped PEMFC bipolar plates", Procedia CIRP 14,Pages 275-280,2014.

[22] Xianguo Li, Imran Sabir, Review of bipolar plates in PEM fuel cells: Flow-field designs, International Journal of Hydrogen Energy 30, Pages 359-371,2005.

[23] Yuh Ming Fernga, Ay Su, "A three-dimensional full-cell CFD model used to investigate the effects of different flow channel designs on PEMFC performance", International Journal of Hydrogen Energy 32, Pages 4466-4476,2007.